Nanoscale

Accepted Manuscript

This article can be cited before page numbers have been issued, to do this please use: G. Yang, T.M. Chen, X. Tian, L. Huang and J. Xiao, *Nanoscale*, 2017, DOI: 10.1039/C7NR05629J.

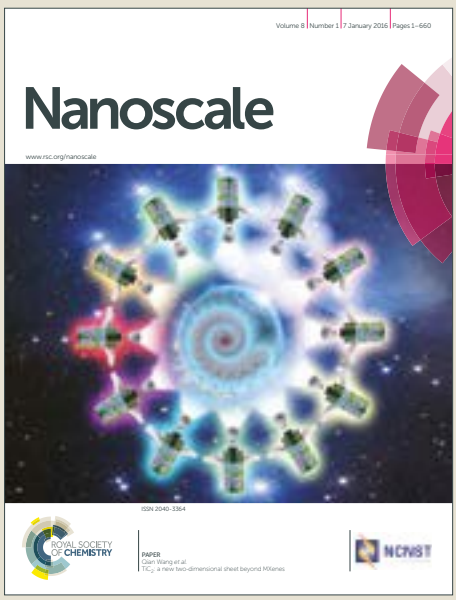

ROYAL SOCIETY OF CHEMISTRY

rsc.li/nanoscale

View Article Online
DOI: 10.1039/C7NR05629J

Nanodiamonds as pH-switchable oxidation and reduction catalysts with enzyme-like activities for immunoassay and antioxidant applications

T. M. Chen [1], X. M. Tian [2], L. Huang [3], J. Xiao [1], G. W. Yang [1]*

[1] *State Key Laboratory of Optoelectronic Materials and Technologies, Nanotechnology Research Center, School of Materials Science & Engineering, School of Physics, Sun Yat-sen University, Guangzhou 510275, Guangdong, P. R. China*

[2] *Department of Biomedical Engineering, Guangzhou Medical University, Guangzhou 510182, P. R. China*

[3] *Department of Histology and Embryology, Zhongshan School of Medicine, Sun Yat-sen University, Guangzhou 510080, P. R. China*

* Corresponding author: stsygw@mail.sysu.edu.cn

View Article Online
DOI: 10.1039/C7NR05629J

Abstract

Nanodiamonds (NDs) have recently become a focus of interest from the viewpoints of both science and technology. Their intriguing properties make them suitable as biologically active substrates, biosensor applications as well as diagnostic and therapeutic biomedical imaging probes. Here, we demonstrate that NDs, as oxidation and reduction catalysts, possess intrinsic enzyme mimetic properties of oxidase, peroxidase and catalase, and these behaviors can be switched by modulating the pH value. NDs not only catalyze the reduction of oxygen (O_2) and hydrogen peroxide (H_2O_2) at acidic pH, but also the dismutation decomposition of H_2O_2 to produce O_2 at alkaline pH. It was proposed that the molecular mechanism of their peroxidase-like activity is electron-transfer acceleration and the source of which is likely deriving from oxygen containing functional groups on their surface. Based on the color reaction, a nanodiamond-based enzyme linked immunosorbent assay (ELISA) was established for the detection of Immunoglobulin G (IgG). Surprisingly, NDs display an excellent antioxidant activity due to the protective effect against H_2O_2-induced cellular oxidative damage. These findings make NDs promising enzyme mimetic candidate and expand applications in biocatalysis, bioassays, and nano-biomedicine.

Keywords: nanodiamond, nanozyme, pH-switchable, ELISA, antioxidant

View Article Online
DOI: 10.1039/C7NR05629J

Introduction

As unique carbon-based nanomaterials, NDs show superior hardness, high thermal conductivity and electrical resistivity, chemical stability, and the resistance to harsh environments[1, 2]. In recent years, NDs have received interest in the biomedical community because of their excellent properties[3, 4]. For instance, they are fluorescent owing to nitrogen vacancies[5], and they have surfaces functionalized[6]. Additionally, they can be produced on large scale via relatively inexpensive synthetic processes[5]. More importantly, toxicity and biocompatibility testing showed that no harmful effects on living organisms were found in these materials[7]. Therefore, NDs have a wide range of potential applications in biomedicine including drug delivery[8, 9], bioimaging and tissue engineering[10, 11]. Herein, we for the first time demonstrate that NDs exhibit multi-enzyme mimetic activity, which can be tuned by pH value. In detail, at acidic condition, they catalyze the reaction of 3,3,5,5-tetramethylbenzidine (TMB) in the presence of H_2O_2 or O_2 to produce a blue color reaction, exhibiting peroxidase-like and oxidase-like activity, respectively. But, at alkaline pH, NDs can catalyze the dismutation decomposition of H_2O_2 accompanied by the formation of O_2, showing the catalase property. The molecular mechanism was established that the oxidase mimetic activity of NDs is induced by their ability to accelerate the electron transfer process between TMB and O_2, while the peroxidase-like activity is originated from them promoting electron transfer from TMB to H_2O_2. Furthermore, we propose that the oxygen containing functional groups on the surface contribute to the source of peroxidase mimetic activity. On the basis of the color reaction, replacing horseradish

View Article Online
DOI: 10.1039/C7NR05629J

peroxidase (HRP) by NDs, an ELISA was developed for the detection of mouse superoxide dismutase (SOD), a classic IgG. Surprisingly, the peroxidase-like activity makes ND an excellent antioxidant against H_2O_2-induced cellular damage, which was employed in an E. coli model. Therefore, these findings make NDs multifunctional nanozyme candidate and pave the way for applications in biocatalysis, bioassays, and nano-biomedicine.

Experimental

Materials preparation

In this case, the nanodiamonds (NDs) were supplied by HeYuan ZhongLian Nanotechnology Co. Ltd (<10nm). They were synthesized by the explosive detonation followed by acid washing. Raw materials were dispersed in water using ultrasonication for 4h to produce suspensions. Three more diamonds from Sigma-Aldrich (<10nm), Element Six Company (~100nm), and Alfa Aesar (40-60 μm) were obtained for control experiments. NaOH, 3,3′,5,5′-Tetramethylbenzidine (TMB), 2-bromo-1-phenylethanone (BrPE), Phenylhydrazine (PH) and albumin from bovine serum (BSA) were purchased from Aladdin Industrial Corporation. Carbamoyl-2,2,5,5-tetramethyl-3-pyrrolin-1-yloxy (CTPO) was purchased from Alfa Aesar. 1,3-Diphenylisobenzofuran (DPBF), phosphate buffered saline (PBS) were purchased from Sigma-Aldrich. Acetic acid, acetic acid sodium salt, Na_2CO_3, $NaHCO_3$, hydrochloric acid, sulfuric acid, nitric acid, hydrogen peroxide (30%), carbon tetrachloride (CCl_4) and anhydrous ethanol were obtained from Guangzhou

View Article Online
DOI: 10.1039/C7NR05629J

Chemical Reagent Factory. Terephthalic acid (TA) was purchased from Tokyo Chemical Industry Co. Ltd. Anti-SOD antibody was obtained from Bioss. Anti-SOD antibody coated microelisa strip plate (12×8strips), mouse superoxide dismutase (SOD), wash solution and stop solution were purchased from Shanghai jijin Chemistry Technology Co. Ltd. Millipore water (18.2 MΩ) was used throughout the experiments. Escherichia coli (E. coli) bacterial strains (ATCC 25922) were obtained from Guangdong Detection Center of Microbiology.

Characterizations

X-ray powder diffraction (XRD) was performed using a Rigaku D/Max-IIIA X-ray diffractometer with Cu Kα radiation (λ = 1.54056 Å, 40 kV, 20 mA) at a scanning rate of 2°/s. Transmission electron microscopy (TEM) and high-resolution TEM (HRTEM) images are acquired by using an FEI Tecnai G2 F30 transition electron microscope equipped with a field-emission gun. The particle size distributions of the colloids were analyzed on a Brookhaven EliteSizer Nanoparticle size-zeta potential and molecular weight analyzer. Ultraviolet-Visible (UV-Vis) absorption spectra of the samples were obtained using a UV 3150 spectrophotometer (Shimadzu, Japan). Fluorescence spectroscopy was performed on Hitachi F-4500 Fluorescence spectrophotometer. A Bruker EQUINOX 55 Fourier transform infrared spectrometer coupled with an infrared microscope (FTIR) was used to determine the functional groups. Wavelength dispersive sequential x-ray fluorescence spectrometry (XRF, Axio^{mAX} Petro) were performed to determine the elemental composition of the samples. The surface analysis was performed by X-ray photoelectron spectroscopy

View Article Online
DOI: 10.1039/C7NR05629J

(XPS) using a Thermo-VG Scientific ESCALAB 250 spectrometer. Photoelectrons were generated by mono Al K α X-ray radiation of energy 1486.6 eV and the calibration was based on the Au 4f with the binding energy at 84.0eV. Electron spin resonance (ESR) spectroscopy measurement was conducted on a Bruker EMX A300 spectrometer equipped with a nitrogen heating setup.

Kinetic analysis

Steady-state kinetic assays for oxidase-like activity were carried by measuring the absorbance change of the NDs/TMB system at 652 nm (ε=39000 $M^{-1}cm^{-1}$) for 5 minutes, using a UV spectrophotometer. Experiments were performed at 25 °C, using 10 mg L^{-1} NDs in a reaction volume of 1 mL 200 mM acetate buffer solution (pH 4.0) with 1mM TMB as substrate. TMB was added to start the reaction, prior to recording the absorbance. Steady-state kinetic assays for peroxidase-like activity were carried by measuring the absorbance change of the NDs/TMB/H_2O_2 system at 652 nm for 5 min. Experiments were performed at 25 °C, using 10 mg L^{-1} NDs in a reaction volume of 1 mL 200 mM acetate buffer solution (pH 4.0) with 1 mM TMB as substrate, and H_2O_2 was 100 mM. TMB was added to start the reaction, prior to recording the absorbance.

The apparent kinetic parameters were calculated based on the Michaelis equation $\upsilon=V_{max}\times[S]/(K_m+[S])$, where υ is the initial velocity, V_{max} is the maximal reaction velocity, [S] is the concentration of the substrate, and K_m is the Michaelis − Menten constant.

Electron spin resonance experiment

View Article Online
DOI: 10.1039/C7NR05629J

ESR spin label oximetry is a quantitative approach to measure oxygen content using spin label CTPO. In the experiments, 0.1 mM CTPO solution was mixed with 100 mM H_2O_2 in carbonate buffer solution (pH 11.0). Followed by addition of 100g L^{-1} NDs and incubation for 3 min, 50 μL sample solutions were put in glass capillary tubes and inserted into the ESR cavity. ESR spectrum was recorded in 2 min. ESR parameter settings were as follows: modulation amplitude 1 G, sweep width 10G, and microwave power 0.19 mW and time constant 40.96 ms.

Detection of singlet oxygen and superoxide anion radical experiments

1,3-Diphenylisobenzofuran (DPBF) was used as a colorimetric and fluorescent probe for detection of singlet oxygen ($^1O_2$) and superoxide anion radical (O_2^-). The standard stock solution (10 μM) of DPBF was made by dissolving in ethanol and was stored at 4 °C in the dark until it was used. Typically, 2.0 mL DPBF solution (10 μM) was mixed with 2 mL acetate buffer solution (200 mM, pH 4.0) and 0.1mL NDs solution (4g L^{-1}). Followed by 12 h incubation in the dark at 37 °C, the resulting solution was centrifuged for absorption and fluorescence analysis. In the fluorescence measurement, the excitation and emission wavelengths were 410 and 455 nm, respectively.

Detection of hydroxyl radicals experiment

Terephthalic acid (TA) was used as a fluorescence probe for tracking of hydroxyl radicals (·OH). In the experiment, a standard solution of sodium salt of TA (Na_2TA) with the concentration of 25 mM was prepared by dissolving 830.7 mg of TA in 200 mL of NaOH (62.5 mM). 0.4 ml of Na_2TA solution was added into a mixture of 3.6

View Article Online
DOI: 10.1039/C7NR05629J

mL acetate buffer solution (200 mM, pH 5.5) with 100 mg L^{-1} NDs and 100 mM H_2O_2. Followed by 12 h incubation in the dark at 25 ℃, the resulting solution was centrifuged for fluorescence measurement. The excitation and emission wavelengths were 315 and 425 nm, respectively.

Cytochrome C electron transfer experiment

Cytochrome C (Cyt C) is an active reactant in electron transfer process and has been used to investigate electron transfer mediator role of NDs. In the experiment, 45 μL of Cyt C (0.4 mM) was added into 170 μL acetate buffer solution (200 mM, pH 4.0) containing 4g L^{-1} NDs. Followed by 12 h incubation in the dark at 25 ℃, the resulting solution was centrifuged for absorption measurement. Furthermore, to evaluate the pH and H_2O_2 effects on Cyt C, its oxidation under acid, neutral and alkaline conditions in the presence of NDs and H_2O_2 were perform, respectively. Typically, 25 μL Cyt C (0.4 mM) was mixed with 5 μL H_2O_2 (320 mM), 45 μL NDs suspension (10 g L^{-1}) and 85 μL buffer solution (pH 4.0, pH 7.0 or pH 10.0). Followed by 15 h incubation in the dark at 25 ℃, the resulting solution was centrifuged for absorption measurement. Control experiments without NDs or H_2O_2 were also performed.

Acid oxidizing treatment of NDs

NDs (40 mg) were dispersed in nitrohydrochloric acid (80 mL) under stirring condition. After standing for 24 h, the mixture was centrifuged (5000 rpm, 5 min) and washed with deionized water for 5 runs. The precipitates were dried at vacuum to give NDs treated by nitrohydrochloric acid (NDs-NA).

View Article Online
DOI: 10.1039/C7NR05629J

NDs-NA were added into the sulfuric acid and nitric acid (3:1, v/v, 80 mL). The mixture was heated at reflux (220 □) for 5 h and then centrifuged (5000 rpm, 5 min) and washed with deionized water. Finally, the NDs were freezed at -50 □ and dried at vacuum for 24 h to give acid-oxidized NDs (NDs-acid).

Chemical titration of oxygen functional groups on NDs

First, 200 mg of BrPE or PH was dissolved in 15 mL CCl_4, and then 20 mg of NDs was added into the solution under stirring condition, standing for about 12 h. Then the precipitates were collected by centrifugation (5000 rpm, 5 min) and washed with CCl_4 for 10 runs. In this procedure for removing CCl_4 solution, the molecules of BrPE and PH selectively reacted with oxygen-containing group on the surface of NDs. Finally, the precipitates were freezed at -50 □ and dried in vacuum for 24 h to give nanodiamond derivatives (ND-BrPE or ND-PH).

Preparation of antibody-NDs conjugates

Antibody (Ab)-NDs conjugates were prepared as follows. First, NDs solution was adjusted by NaOH to be around pH 9.0. Then 20 μL stock solution of anti-SOD antibody (1mg/mL) was introduced and incubated at 4 ºC over night. Followed by adding blocking buffer (1% BSA in PBS buffer) to passivate remaining sites of NDs, excess amount of antibody and BSA was removed by centrifugation (10000 rpm, 10 min) for two runs. The resulting pellet was dispersed in 500 μL PBS solution and stored at 4 ºC for further use.

Immunoassay

The sandwich immunoassay was carried out on an anti-SOD antibody coated

View Article Online
DOI: 10.1039/C7NR05629J

96-well microtiter plate. Firstly, 50 μL SOD standard solution at different concentrations were added to the wells. Subsequently, the plate was incubated at 37 °C for 1 h with 100 μL of the Ab-NDs conjugates. After washing 3 times with wash buffer, 100 μL substrate solution (pH 4.0) containing TMB (1 mM) and H_2O_2 (100 mM) was added into each well. The plate was incubated at 37 °C for 20 min. 50 μL stop solution was added to stop the reaction and displayed a final yellow color. The ELISA reading was performed at 450 nm by a plate microreader.

Bacterial culture and antioxidant experiments

Monocolony of E. coli on the solid Luria-Bertani (LB) agar plate was transferred to 20 mL of liquid LB culture medium and grown at 37 °C for 12 h under 180 rpm rotation. Then the bacteria were diluted with broth to 10^5 cfu mL^{-1}. The as-prepared bacteria solution (500 μL) was mixed with NDs (500mg L^{-1}) , H_2O_2 (0.1%) and acetate buffer solution (pH 5.5) for 30 min. Then the solution was placed on solid medium by spread plate method and cultured for 24 h before observing the number of the bacteria colonies via counting by naked eye and OD600 measurement, respectively. Control experiments were performed in parallel without H_2O_2 or NDs.

Results and Discussion

Characterization of NDs

The XRD pattern of the sample in Fig. 1a demonstrates the presence of diamond (JCPDS No. 75-0219). The corresponding transmission electron microscopy (TEM) analysis in Fig. 1b shows that NDs are of irregular-particle shape. According to TEM

View Article Online
DOI: 10.1039/C7NR05629J

data, a statistical analysis of 200 particles indicated that the diameter of NDs is mainly distributed in 2-10 nm with the average size of 5.6 nm. Fig. 1c and d show the High-resolution TEM (HRTEM) and selected area electron diffraction (SAED) images of NDs, respectively. Three strong di□raction rings represent the (111), (220), and (311) planes of diamond, further confirming the presence of NDs[12]. The particle size distribution of the resultant suspension was monitored by dynamic light scattering (DLS) measurements. The peak of the particle size distribution located at around 85 nm, as shown in Fig. S1a.

Oxidase-like and peroxidase-like activities of NDs

To investigate oxidase-like and peroxidase-like activities of NDs, color reaction was performed in the absence and presence of H_2O_2, choosing TMB as the substrate. First, the NDs can catalyze the oxidation of TMB by dissolved O_2 in water, producing light blue color for TMB (maximum absorbance at 652 nm). In contrast, the solutions without NDs showed no color change. This result indicates that the NDs have oxidase-like activity[13]. Next, the effect of H_2O_2 on TMB oxidation was investigated. By addition of H_2O_2, the color evolution TMB oxidation was much faster and exhibited deeper color at the same time intervals. Similarly, the control experiments without NDs also showed negligible color variation (Fig. 2a).

Other control experiments with three more diamonds from different sources were incubated under the standard reaction conditions over a period of 10 min. As shown in Fig. S2a, similar results were obtained showing the generality of NDs in the peroxidase-like properties. Furthermore, diamond crystal powders, 40-60 μm, with

View Article Online
DOI: 10.1039/C7NR05629J

uncovered surface show negligible peroxidase-like activity, suggesting that the peroxidase-like activity of NDs is likely to attribute to their nanoscale effect (Fig. S2c and d).

It is important to rule out the possibility that the observed activity is caused by leaching of ions into acidic solution. To test this, we incubated NDs in the standard reaction buffer for 10 min and then removed the NDs from solution by centrifugation. We then compared the activity of the supernatant with that of NDs under the same conditions. As shown in Fig. S2b, the supernatant had no activity, showing that the observed peroxidase-like activity is due to intact NDs. These results above indicates that the NDs possess peroxidase-like toward the typical peroxidase substrate[14].

Note that, the catalytic activities of NDs are similar to natural oxidase and peroxidase, depending on pH and temperature (Fig. 2b and c)[13, 14]. They were measured while varying pH from 1.5 to 7.0, temperature from 25°C to 60°C. The results indicate that both of them showing optimal pH at 4.0 and a suitable temperature at around 35°C.

The apparent steady-state kinetics is investigated for the reaction catalyzed by NDs. Similar to the enzyme-catalyzed reaction, the typical Michaelis–Menten curves are observed for NDs with and without H_2O_2 (Fig. 2d and e)[13, 14]. Kinetic parameters are obtained by fitting to the Michaelis–Menten model. Results in Table 1 show that in comparison with other reported nanomaterials with oxidase-like activities, NDs has lower K_m value for TMB in the absence of H_2O_2, indicating that a lower TMB concentration was required to achieve maximal activity for NDs[13, 15]. In the presence

View Article Online
DOI: 10.1039/C7NR05629J

of H_2O_2, the NDs have lower K_m value than HRP. On the other hand, the apparent K_m value of NDs with H_2O_2 as the substrate is also lower than HRP and many other nanozymes, suggesting that NDs have a higher affinity[14, 16-19].

Catalase-like activity of NDs

Similar to catalase, NDs are capable of catalyzing the degradation of H_2O_2 to produce O_2. With the involvement of NDs, the H_2O_2 decomposed violently and the O_2 bubbles could be clearly seen by naked eyes. In contrast, the control experiments without NDs or H_2O_2 showed negligible bubbles (Fig. 3a). To further evaluate the catalase-like activity of NDs, ESR spin oximetry with respect to the product O_2 in the reaction was conducted. This measurement is based on the bimolecular collision of oxygen molecule with a spin probe, in which the high O_2 concentration is accompanied by a decrease in the peak height of the ESR signal[20]. As shown in Fig. 3b, the decrease in the peak intensity with time was observed, indicating the enhanced production of O_2 in the H_2O_2 degradation reaction catalyzed by NDs[21, 22]. Fig. 3c shows that the strong dependence between catalytic activity of NDs and H_2O_2 concentration. All these results provide direct evidence supporting that NDs behave like catalase[19, 23]. We also investigated the e□ect of pH and temperature on the catalytic activity of NDs. Fig. 3d and e show that catalase-like activity of NDs increases with rising pH and temperature up to pH 11 and 60 □, respectively. In contrast, the natural catalase is quite sensitive to pH and temperature, showing decreased activity in high pH and high temperature. Hence, the higher stability of NDs makes them promising catalase mimic particularly in extreme conditions.

View Article Online
DOI: 10.1039/C7NR05629J

Accordingly, these results above suggest that NDs exhibit multi-enzyme mimetic activity, which can be tuned by modulating pH value. At acidic pH, they catalyze the reaction of TMB in the presence of H_2O_2 or O_2 to produce a blue color reaction, showing peroxidase-like and oxidase-like activity, respectively. On the other hand, they catalyze the dismutation decomposition of H_2O_2 accompanied by the formation of O_2 at alkaline pH, showing catalase property (Fig. 3f). Therefore, NDs are pH-controllable multifunctional nanozyme.

Molecular mechanism of oxidase-like and peroxidase-like activity of NDs

Generally, the catalytic pathways of oxidase-like and peroxidase-like activity can be sorted into the generation of reactive oxygen species (ROS) or the electron transfer process[21]. To evaluate the possible active intermediate in the present system, various fluorescent and colorimetric probes were employed. 1,3-Diphenylisobenzofuran(DPBF) was used as a probe for detection of singlet oxygen ($^1O_2$) and superoxide anion radical (O_2^-) by decrease in the intensity of its absorption and fluorescence[15, 24, 25]. Fig. 4a shows the absorption and fluorescence change in the mixed solution of DPBF and NDs. After 12 h reaction, compared with control experiments, negligible absorption and fluorescence decrease were observed, indicating the absence of $^1O_2$ and O_2^- in the oxidase-like catalytic process. Furthermore, Terephthalic acid (TA) is used as a fluorescence probe for tracking of hydroxyl radicals (·OH) because it could capture ·OH and generate 2-hydroxyterephthalic acid, emitting the unique fluorescence around 425 nm[26]. After 12 h reaction, the fluorescence in the solution containing TA, NDs and H_2O_2 is lower

View Article Online
DOI: 10.1039/C7NR05629J

than mixture of TA and H_2O_2. In addition, TA did not show fluorescence upon incubation with NDs (Fig. 4b). This results exclude the generation of ·OH during the oxidase-like and peroxidase-like catalysis[27].

To verify the NDs mediated electron transfer process from TMB to O_2 (or H_2O_2), cytochrome C (Cyt C) was used to test the accepting electron ability of NDs because Cyt C is an active reactant in the electron transfer process[28]. While incubated with NDs, absorbance of Cyt C at 520 and 550 nm gradually decreased with the evolution of a new peak at 530 nm (Fig. 4c). The corresponding change from reduced state to oxidized state for Cyt C clearly indicates electron transfer from Cyt C to NDs[21]. The pH effects on Cyt C oxidation were also investigated. The results show that NDs can accept electron from Cyt C over a wide pH range. Also, the disappearance of absorbance band of Cyt C is associated with the ultrahigh ability of combination of NDs and H_2O_2 to accelerate the Cyt C oxidation (Fig. S5 a-c).

Therefore, all the above results proposed the mechanism of NDs acting as oxidase and peroxidase (Fig. 4d). First, TMB binds to the hydrophobic domains on surface of NDs, the amino group of which donates lone-pair electrons to NDs, leading to increased electron density of NDs. Second, electron-rich NDs transfer electrons to close-by dissolved O_2 (or H_2O_2) molecules, which further accelerates the electron transfer process between NDs and TMB. Finally, during this catalytic cycle, TMB is oxidized into blue derivative while O_2 (or H_2O_2) are reduced to water in acidic condition[21, 26, 29]. The reaction pathways can be described by the following two equations for O_2 and H_2O_2 as electron acceptors[23], respectively:

View Article Online
DOI: 10.1039/C7NR05629J

$$O_2 + 4H^+ + 4e^- = 2H_2O \quad (1)$$

$$H_2O_2 + 2H^+ + 2e^- = 2H_2O \quad (2)$$

In a word, the oxidase mimetic activity of NDs is induced by their ability to accelerate the electron transfer process between TMB and O_2, while the peroxidase-like activity is originated from them promoting electron transfer from TMB to H_2O_2.

Source of the peroxidase mimetic activity

One of the key concerns in identifying and describing metal-free catalysis is the suspected influence of metal impurities in the catalyst. Commercial NDs were prepared with metal catalysts, which inevitably remain as metal contaminants. Post-treatment by acid washing effectively removed the residual metals to a great extent. X-ray fluorescence spectrometry (XRF) reveals that the residual metals in the tested NDs were very low (Table 2). Additionally, there is no signal of metals in the surface layer at the limit of detection by x-ray photoelectron spectroscopy (XPS) (Fig. 5f). This difference suggests that if there is residual metal, it must be embedded in the carbon and not exposed to the reactants. This explanation is supported by the XRF of the NDs treated by nitrohydrochloric acid (NDs-NA), which shows negligible difference to that of raw NDs. Therefore, the reactivity originated exclusively from metal-free active sites on NDs and that residual metals played no positive role.

According to the HRTEM image in Fig. 5a, agglomerated NDs are covered with some amorphous carbon[30]. However, no signal of the amorphous carbon was detected in the XRD pattern, indicating that they are at low content. To reduce the amorphous carbon on the surface of NDs, NDs-NA were further treated with refluxing in strong

View Article Online
DOI: 10.1039/C7NR05629J

acid to give acid-oxidized NDs (NDs-acid) (Fig. 5b)[31-36]. Further, kinetic assays were performed to evaluate the influence of amorphous carbon in the peroxidase-like activity. The results show that NDs-acid possess higher peroxidase-like activity than NDs-raw, suggesting the possibility that the amorphous carbon inhibiting the catalysis. However, after acid oxidizing treatment, the oxygen containing functional groups on the surface of NDs also changed according to the Fourier transform infrared (FT-IR) spectroscopies shown in Fig. S7. For this reason, their contribution to increase in catalytic activity cannot be excluded. A detailed discussion is given below. In addition, Comparison experiment of peroxidase kinetic spectrums of ultrasound-treated and untreated NDs were performed, respectively, under the same conditions (Fig. S1b). Interestingly, we found limited influence of aggregation on peroxidase kinetic process and peroxidase-like activity.

Present research on carbon-based catalysis implies that oxygen containing functional groups may act as the catalytic active sites for oxidation and reduction reaction[37]. It is believed that such surface groups facilitate the charge transfer between the carbon nanomaterials and substrates. Herein, through selectively deactivating these specific functional groups and investigating the catalytic activity of different derivatives of NDs, the role they played as peroxidase mimics can be investigated evidently[26, 38]. The raw materials of NDs (NDs-raw) were mainly covered with carbonyl (-C=O) and carboxylic (-COOH) on their surface according to the FT-IR spectroscopy and O 1s XPS spectra (Fig. 5c and d). Phenylhydrazine (PH) and 2-bromo-1-phenylethanone (BrPE) were chosen as the titrants to specifically react

View Article Online
DOI: 10.1039/C7NR05629J

with the -C=O and -COOH groups on the NDs, respectively (Fig. 5g)[26, 38]. The FT-IR spectrums of NDs treated with BrPE and PH exhibit a significant decrease of the C=O signal suggesting the successful deactivation of -C=O and -COOH to produce derivatives of NDs (NDs-PE and NDs-BrPE, respectively) (Fig. 5e)[12, 26, 39]. To evaluate their peroxidase-like activity, kinetic assays were also conducted. As shown in Fig. 5f, under the same conditions, the peroxidase-like activity of NDs-PE and NDs-BrPE are lower than that of NDs-raw, which indicate a positive correlation between the concentration of -C=O and -COOH groups and the activity. In addition, the FT-IR spectrums of NDs also show the presence of -OH group in H_2O or H_3O^+ (Fig. 5c). To evaluate the contribution to peroxidase-like activity of this group, two NDs from different sources showing completely same signal intensity of -OH group were employed to perform color reaction (Fig. S6). However, Fig. S2a shows the significant color variation indicating that the peroxidase-like activity is irrelevant to -OH groups in H_2O or H_3O^+. Recently, calculations suggest that the pre-adsorbed -OH groups on the surfaces of noble metal nanoparticles, which are only favorably formed in basic conditions, trigger the switch between activities of peroxidase and catalase and render the pH-switchability[40]. The pre-adsorbed -OH groups on the surface of NDs may also serve as switchers for catalytic activities.

We also discussed the influence of nitrogen species on their catalytic activity. Fig. S3 shows the representative bonding configurations for N in carbon materials: pyridinic N, pyrrolic N, graphitic N and pyridine-N-oxide. Recently, experimental and theoretical studies indicated that pyridinic N plays a more important role than other

View Article Online
DOI: 10.1039/C7NR05629J

nitrogen species in catalyzing redox reaction[41-43]. However, in our studies, the XPS results for NDs illustrate the nitrogen content is only 2 at % and the N 1s spectrum can be deconvoluted into the following two peaks: 400.2 eV and 403.5 eV, which are assigned to pyrrolic nitrogen and pyridine-N-oxide, respectively (Fig. S41 and 2). Based on the above results, we proposed that nitrogen species have almost no influence on the enzyme like property.

Accordingly, we obtained the evidence that the embedded metal impurities have no effect on the catalysis, whereas the covered amorphous carbon probably inhibit this reaction, and the peroxidase-like activity of NDs is likely to derive from -C=O and -COOH groups on the surface. Further research is needed in the future to determine the other origin of the activity.

Application in immunoassay

The NDs were employed in a traditional HRP-based ELISA by using them in the place of HRP. Synthesized by the explosive detonation and washed by strong acid, NDs have surface functionalized with a lot of active groups[2]. It provides a convenient way for binding of antibody without needing other modifications. Mouse SOD was chosen as antigen model for immunoassay detection. SOD is an enzyme found in all aerobic cells, which plays a critical role in reducing the oxidative damage and inflammation. Its levels in the body are associated with the health condition. Hence, the detection of SOD provides great help in disease diagnosis[44, 45]. Fig. 6a illustrates the construction of sandwich immunoassay format for SOD detection. In this assay, NDs served as HRP, not only binding with the detection antibodies, but also

View Article Online
DOI: 10.1039/C7NR05629J

catalyzing the color reaction of TMB and H_2O_2. Fig. 6b displays the ELISA results, which showed the absorbance at 450 nm was dependent on the concentration of SOD. The results indicate the successful attachment of Ab to NDs and robustness of the assay for bio-detection. These results demonstrate the versatility of NDs as a detection tool due to their unique oxidase-like and peroxidase-like activities, which allows them for the potential application in the specific measurements of various antigens by NDs-based ELISA kits and in other biodetections.

Application in antioxidation

H_2O_2 is a common reactive ROS produced in cellular metabolism, such as glucose oxidation catalyzed by glucose oxidase and superoxide anion radical scavenging by SOD[46, 47]. In nature, catalase and peroxidase have been evolved to protect cells against H_2O_2-induced oxidative damage[47]. However, in Alzheimer's disease or other pathological cases, cells may reduce or even lose their abilities to decompose H_2O_2, leading to serious DNA and protein structure damage[48]. In our case, NDs with peroxidase-like activities can be speculated to protect cells against H_2O_2-induced oxidative damage. E. coli was used as a cell model.

Plate count method for counting number of bacterial colonies was applied to evaluate the antioxidant activity of NDs against E. coli[49]. Fig. 7a shows that treating E. coli with 1% H_2O_2 for 24h resulted in almost completely death of cells. However, incubation of cells with 0.5mg/ml NDs and 1% H_2O_2 for 24h lead to significantly enhanced cell proliferation. As we know, NDs show peroxidase activity in the presence of H_2O_2 at acidic pH, catalyzing reduction of H_2O_2 by promoting electron

View Article Online
DOI: 10.1039/C7NR05629J

transfer instead of producing ·OH. The peroxidase property provides protective effect of NDs on cellular oxidative damage induced by H_2O_2 in culture medium. On the other hand, in the case that NDs show oxidase activity, no harmful ROS for bacterial cells were produced. Furthermore, without addition of H_2O_2, NDs also showed the excellent protective activity for E. coli implying that NDs could inhibit the oxidant effect of endogenous H_2O_2 in E. coli. To further confirm the antioxidant function of NDs, OD600 measurement was also employed for estimating density of bacteria cell in a medium (Fig. 7b)[15]. The results are highly consistent with that of the experiments above. Simultaneously, the influence of NDs on the growth of E. coli could be clearly observed via the numbers of bacterial colonies on the plates (Fig. 7c-f). In the basis of their enzyme mimetic activity, NDs display excellent performance on inhibiting H_2O_2-induced Oxidative damage, which make them promising drug candidates for preventing a wide range of diseases including Alzheimer's disease, Parkinson's disease, the pathologies caused by diabetes and so on[47].

Conclusion

In summary, we have demonstrated that NDs exhibit multi-enzyme mimetic activity, which can be tuned by adjusting pH value. At acidic condition, they catalyze the reaction of TMB in the presence of H_2O_2 or O_2 to produce a blue color reaction, showing peroxidase-like and oxidase-like activity, respectively. On the other hand, at alkaline pH, they catalyze the dismutation decomposition of H_2O_2 to produce O_2, showing catalase property. The Michaelis-Menten kinetics indicated that NDs has

View Article Online
DOI: 10.1039/C7NR05629J

higher affinity than HRP and many other nanomaterials with oxidase-like or peroxidase-like activities. The molecular mechanism of the catalytic reaction was also investigated, which exhibiting that the oxidase mimetic activity of NDs is induced by their ability to accelerate the electron transfer process between TMB and O_2, while the peroxidase-like activity is originated from them promoting electron transfer from TMB to H_2O_2. Furthermore, several experiments on the source of peroxidase-like activity confirm the positive contribution from -C=O and -COOH groups on the surface. In addition, the color reaction was used to develop an ELISA for the detection of SOD, replacing horseradish HRP by NDs. Surprisingly, the peroxidase-like and oxidase-like properties offer NDs excellent protective e□ect against H_2O_2-induced oxidant damage in an E. coli model. Therefore, these results make NDs multifunctional nanozyme candidate and find more novel applications in nano-biotechnology.

Acknowledgements

The National Basic Research Program of China (2014CB931700), the National Natural Science Foundation of China (91233203), the National Science Foundation for Young Scholars of China (81401462) and State Key Laboratory of Optoelectronic Materials and Technologies supported this work. We thank Q. M. Liu from South China Normal University for enzyme kinetic assay assistance. We also thank X. Y. Guo and T. L. Sun from Guangdong Detection Center of Microbiology for bacterial culture and antioxidant experiment assistance.

View Article Online
DOI: 10.1039/C7NR05629J

References

1 V. V. Danilenko, *Phys. Solid State*, 2004, **46**, 595-599.

2 V. N. Mochalin, O. Shenderova, D. Ho and Y. Gogotsi, *Nature Nanotech.*, 2012, **7**, 11-23.

3 S. Wang, R. Cazelles, W. C. Liao, M. Vazquez-Gonzalez, A. Zoabi, R. Abu-Reziq and I. Willner, *Nano Lett.*, 2017, **17**, 2043-2048.

4 M. Vázquez-González, W.-C. Liao, R. Cazelles, S. Wang, X. Yu, V. Gutkin and I. Willner, *ACS Nano*, 2017, **11**, 3247-3253.

5 Y.-R. Chang, H.-Y. Lee, K. Chen, C.-C. Chang, D.-S. Tsai, C.-C. Fu, T.-S. Lim, Y.-K. Tzeng, C.-Y. Fang, C.-C. Han, H.-C. Chang and W. Fann, *Nature Nanotech.*, 2008, **3**, 284-288.

6 Q. Zhang, V. N. Mochalin, I. Neitzel, I. Y. Knoke, J. Han, C. A. Klug, J. G. Zhou, P. I. Lelkes and Y. Gogotsi, *Biomaterials*, 2011, **32**, 87-94.

7 N. Mohan, C. S. Chen, H. H. Hsieh, Y. C. Wu and H. C. Chang, *Nano Lett.*, 2010, **10**, 3692-3699.

8 E. K. Chow, X. Q. Zhang, M. Chen, R. Lam, E. Robinson, H. Huang, D. Schaffer, E. Osawa, A. Goga and D. Ho, *Sci. Transl. Med.*, 2011, **3**, 772-778.

9 C. M. Jimenez, N. Z. Knezevic, Y. G. Rubio, S. Szunerits, R. Boukherroub, F. Teodorescu, J. G. Croissant, O. Hocine, M. Seric and L. Raehm, *J. Mater. Chem. B*, 2016, **4**, 5803-5808.

10 T. J. Wu, Y. K. Tzeng, W. W. Chang, C. A. Cheng, Y. Kuo, C. H. Chien, H. C. Chang and J. Yu, *Nature Nanotech.*, 2013, **8**, 682-689.

View Article Online
DOI: 10.1039/C7NR05629J

11 V. N. Mochalin, I. Neitzel, B. J. M. Etzold, A. Peterson, G. Palmese and Y. Gogotsi, *ACS Nano*, 2011, **5**, 7494-7502.

12 J. Xiao, G. Ouyang, P. Liu, C. X. Wang and G. W. Yang, *Nano Lett.*, 2014, **14**, 3645-3652.

13 A. Asati, S. Santra, C. Kaittanis, S. Nath and J. M. Perez, *Angew. Chem. Int. Ed.*, 2009, **48**, 2308-2312.

14 L. Gao, J. Zhuang, L. Nie, J. Zhang, Y. Zhang, N. Gu, T. Wang, J. Feng, D. Yang, S. Perrett and X. Yan, *Nature Nanotech.*, 2007, **2**, 577-583.

15 Y. Tao, E. Ju, J. Ren and X. Qu, *Adv. Mater.*, 2015, **27**, 1097-1104.

16 R. André, F. Natálio, M. Humanes, J. Leppin, K. Heinze, R. Wever, H. C. Schröder, W. E. G. Müller and W. Tremel, *Adv. Funct. Mater.*, 2011, **21**, 501-509.

17 Y. Lin, J. Ren and X. Qu, *Acc. Chem. Res.*, 2014, **47**, 1097-1105.

18 J. Mu, Y. Wang, M. Zhao and L. Zhang, *Chem. Commun. (Camb.)*, 2012, **48**, 2540-2542.

19 J. Fan, J. J. Yin, B. Ning, X. Wu, Y. Hu, M. Ferrari, G. J. Anderson, J. Wei, Y. Zhao and G. Nie, *Biomaterials*, 2011, **32**, 1611-1618.

20 C. S. Lai and S. Lukiewicz, *Proc. Natl. Acad. Sci. USA*, 1982, **79**, 1166-1170.

21 H. Su, D. D. Liu, M. Zhao, W. L. Hu, S. S. Xue, Q. Cao, X. Y. Le, L. N. Ji and Z. W. Mao, *ACS Appl. Mater. Interfaces*, 2015, **7**, 8233-8242.

22 W. He, Y. T. Zhou, W. G. Wamer, X. Hu, X. Wu, Z. Zheng, M. D. Boudreau and J. J. Yin, *Biomaterials*, 2013, **34**, 765-773.

View Article Online
DOI: 10.1039/C7NR05629J

23 W. He, Y. Liu, J. Yuan, J. J. Yin, X. Wu, X. Hu, K. Zhang, J. Liu, C. Chen, Y. Ji and Y. Guo, *Biomaterials*, 2011, **32**, 1139-1147.

24 A. F. Schwerin, J. C. Johnson, M. B. Smith, P. Sreearunothai, D. Popović, J. Cerný, Z. Havlas, I. Paci, A. Akdag and M. K. Macleod, *J. Phys. Chem. A*, 2010, **114**, 1457-1473.

25 T. Ohyashiki, M. Nunomura and T. Katoh, *Biochim. Biophys. Acta*, 1999, **1421**, 131-139.

26 H. Sun, A. Zhao, N. Gao, K. Li, J. Ren and X. Qu, *Angew. Chem. Int. Ed.*, 2015, **54**, 7176-7180.

27 T. M. Chen, J. Xiao and G. W. Yang, *RSC Adv.*, 2016, **6**, 70124-70132.

28 J. Dong, L. Song, J. J. Yin, W. He, Y. Wu, N. Gu and Y. Zhang, *ACS Appl. Mater. Inter.*, 2014, **6**, 1959-1970.

29 Y. Song, K. Qu, C. Zhao, J. Ren and X. Qu, *Adv. Mater.*, 2010, **22**, 2206-2210.

30 M. Ozawa, M. Inaguma, M. Takahashi, F. Kataoka, A. Krueger and E. Ōsawa, *Adv. Mater.*, 2007, **19**, 1201-1206.

31 K. Y. Niu, H. M. Zheng, Z. Q. Li, J. Yang, J. Sun and X. W. Du, *Angew. Chem. Int. Ed.*, 2011, **50**, 4099-4102.

32 E. Ōsawa, *Diam. Relat. Mater.*, 2007, **16**, 2018-2022.

33 A. Krueger, *J. Mater. Chem.*, 2008, **18**, 1485-1492.

34 J. P. Boudou, P. A. Curmi, F. Jelezko, J. Wrachtrup, P. Aubert, M. Sennour, G. Balasubramanian, R. Reuter, A. Thorel and E. Gaffet, *Nanotechnology*, 2009, **20**, 235602.

View Article Online
DOI: 10.1039/C7NR05629J

35 I. Aharonovich, C. Zhou, A. Stacey, F. Treussart, J.-F. Roch and S. Prawer, *Appl. Phys. Lett.*, 2008, **93**, 243112.

36 Y. R. Chang, H. Y. Lee, K. Chen, C. C. Chang, D. S. Tsai, C. C. Fu, T. S. Lim, Y. K. Tzeng, C. Y. Fang, C. C. Han, H. C. Chang and W. Fann, *Nat. Nanotechnol.*, 2008, **3**, 284-288.

37 E. Y. Mironova, M. Ermilova, M. Efimov, L. Zemtsov, N. Orekhova, G. Karpacheva, G. Bondarenko, N. Zhilyaeva, D. Muraviev and A. Yaroslavtsev, *Russ. Chem. Bull.*, 2013, **62**, 2317-2321.

38 W. Qi, W. Liu, B. Zhang, X. Gu, X. Guo and D. Su, *Angew. Chem. Int. Ed.*, 2013, **52**, 14224-14228.

39 J. Xiao, P. Liu, L. Li and G. Yang, *J. Phys. Chem. C*, 2015, **119**, 2239-2248.

40 J. Li, W. Liu, X. Wu and X. Gao, *Biomaterials*, 2015, **48**, 37-44.

41 Y. Lin and D. Su, *ACS nano*, 2014, **8**, 7823-7833.

42 H. B. Yang, J. Miao, S.-F. Hung, J. Chen, H. B. Tao, X. Wang, L. Zhang, R. Chen, J. Gao and H. M. Chen, *Science Adv.*, 2016, **2**, e1501122.

43 D. Guo, R. Shibuya, C. Akiba, S. Saji, T. Kondo and J. Nakamura, *Science*, 2016, **351**, 361-365.

44 M. Hayyan, M. A. Hashim and I. M. AlNashef, *Chem. Rev.*, 2016, **116**, 3029-3085.

45 Y. Sheng, I. A. Abreu, D. E. Cabelli, M. J. Maroney, A. F. Miller, M. Teixeira and J. S. Valentine, *Chem. Rev.*, 2014, **114**, 3854-3918.

46 A. S. G. Huggett and D. A. Nixon, *Lancet*, 1957, **273**, 368-370.

View Article Online
DOI: 10.1039/C7NR05629J

47 M. Giorgio, M. Trinei, E. Migliaccio and P. G. Pelicci, *Nat. Rev. Mol. Cell Bio.*, 2007, **8**, 722-728.

48 R. A. Roberts, R. A. Smith, S. Safe, C. Szabo, R. B. Tjalkens and F. M. Robertson, *Toxicology*, 2010, **276**, 85-94.

49 E. Goldman and L. H. Green, *Practical Handbook of Microbiology, Second Edition*, CRC Press, 2009.

View Article Online
DOI: 10.1039/C7NR05629J

Table 1 Comparison of the kinetic parameters of NDs and HRP. K_m is the Michaelis constant, V_{max} is the maximal reaction velocity.

Catalyst	Substrate	K_m (mM)	V_{max} (M s^{-1})	References
HPR	TMB	0.434	1.00×10^{-7}	12
	H_2O_2	3.70	8.71×10^{-8}	
NDs	TMB	0.115	7.11×10^{-9}	This work
	H_2O_2	0.752	2.09×10^{-9}	
NDs	TMB	0.103	2.80×10^{-10}	This work

Table 2 Stoichiometry composition for NDs obtained by XRF.

Metal compound	Concentration (%)	
	NDs	NDs-NA
Na	0.078	0.024
Mg	0.007	0
Fe	0.006	0.003
Al	0.006	0.006
Ca	0.005	0.008

View Article Online
DOI: 10.1039/C7NR05629J

Figure Captions

Figure 1. (a) XRD pattern of NDs. All reflection peaks can be indexed to diamond. (b) TEM image of NDs. The insert shows the size distribution analysis from 200 random particles. (c) HRTEM image of NDs. (d) Corresponding SAED pattern of NDs.

Figure 2. NDs show the oxidase-like and peroxidase-like activities. (a) The NDs catalyzes the oxidation of TMB, in the presence of dissolved O_2 or H_2O_2. 1) TMB, 2) NDs, 3) NDs+ H_2O_2, 4) TMB+ H_2O_2, 5) TMB+ NDs, 6) TMB+ H_2O_2 +NDs. (b and c) The oxidase-like activity of NDs is pH and temperature dependent, showing an optimal pH of 3.0 - 4.5 and temperature around 25 - 35□. Experiments were carried out using 10 μg NDs in a reaction volume of 1 mL, in acetate buffer, with 1 mM TMB as substrate. The peroxidase-like activity of NDs is pH and temperature dependent, showing an optimal pH of 3.5 - 4.5 and temperature around 35□. Experiments were carried out using 10 μg NDs in a reaction volume of 1 ml, in acetate buffer, with 1 mM TMB and 100 mM H_2O_2 as substrates. The maximum point in each curve (b and c) was set as 100%. (d and e) Apparent steady-state kinetic study of NDs. The velocity (v) of the reaction was measured using 10 μg NDs in 1 ml of phosphate pH 4.0 at 25°C. (d) The concentration of dissolved O_2 was fixed and the TMB concentration was varied. The concentration of H_2O_2 was 100mM and the TMB concentration was varied. (e) The concentration of TMB was 1mM and the H_2O_2 concentration was varied.

View Article Online
DOI: 10.1039/C7NR05629J

Figure 3. (a-e) The catalase-like activity of NDs. (a) Gas bubbles were observed after incubation of 100 mM H_2O_2 and 10 mg L^{-1} NDs in carbonate bu□er (pH 11.0) for 5min. ESR spectra of CTPO show that the catalase-like activity of NDs is dependent on pH (b), temperature (c) and H_2O_2 concentration (d). (e) The O_2 production in this system is time dependent. (f) The enzyme mimetic activity of NDs is pH switchable. NDs show oxidase-like and peroxidase-like activity in acidic pH and catalase-like activity in alkaline pH.

Figure 4. Mechanism of oxidase-like and peroxidase-like activities of NDs. (a) UV-Vis absorption spectra and fluorescence spectra for DPBF incubated with NDs. (b) Fluorescence spectra for interaction of TA with NDs. (c) UV-Vis absorption spectra for Cyt C incubated with NDs. (d) Proposed mechanism for the oxidase-like and peroxidase-like activity of NDs.

Figure 5. (a) TEM image of raw NDs and corresponding HRTEM image. (b) TEM image of NDs-acid and corresponding HRTEM image. (c) FTIR spectra of NDs, NDs-BrPE and NDs-PH. The absorption peak at 1730 cm^{-1} belongs to the C=O groups. (d) High-resolution O 1s XPS spectrum of NDs. (e) Schematic of selective deactivation of -C=O and -COOH groups on the surface of NDs. (f) Comparison of peroxidase kinetic spectrums of NDs-raw, NDs-acid, NDs-BrPE and NDs-PH, respectively, under the same conditions.

View Article Online
DOI: 10.1039/C7NR05629J

Figure 6. (a) The construction of NDs-based sandwich immunoassay format. (2) NDs-based ELISA is sensitive to the concentration of mouse SOD.

Figure 7. (a) Number of colonies of E. coli treated with 0.5mg/ml NDs and/or 1% H_2O_2. (b) Optical density at 600 nm (OD600) of bacterial suspension of E. coli treated with 0.5mg/ml NDs and/or 1% H_2O_2. (c-f) Representative digital images show the influence of NDs on the growth of E. coli bacterial.

View Article Online
DOI: 10.1039/C7NR05629J

Figure 1

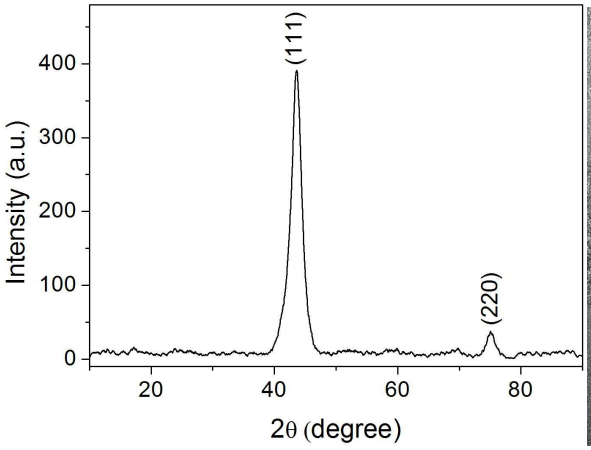

(a)

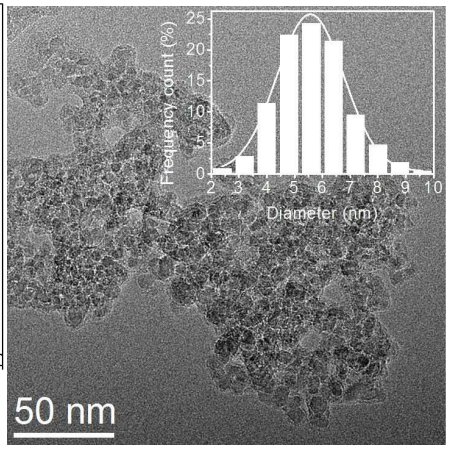

(b)

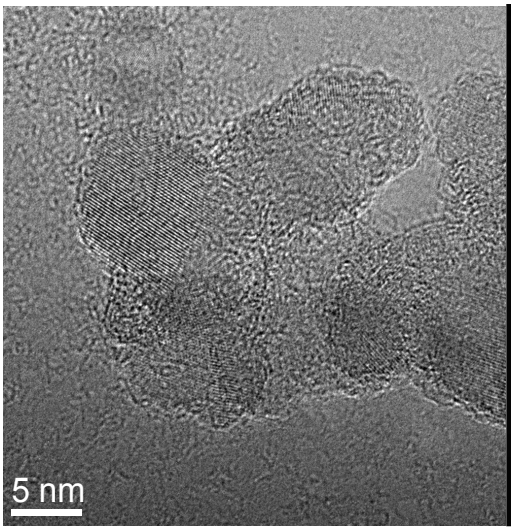

(c)

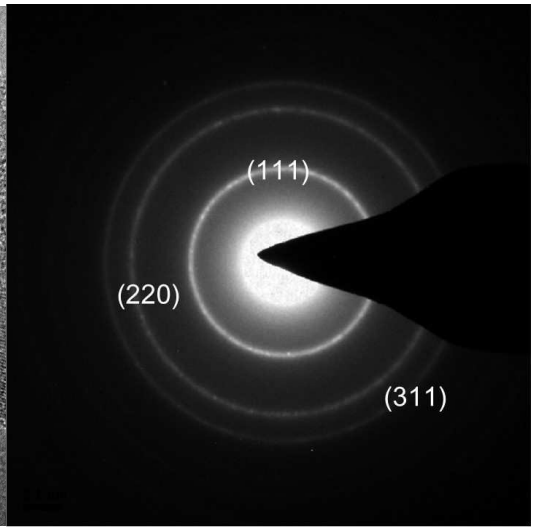

(d)

View Article Online
DOI: 10.1039/C7NR05629J

Figure 2

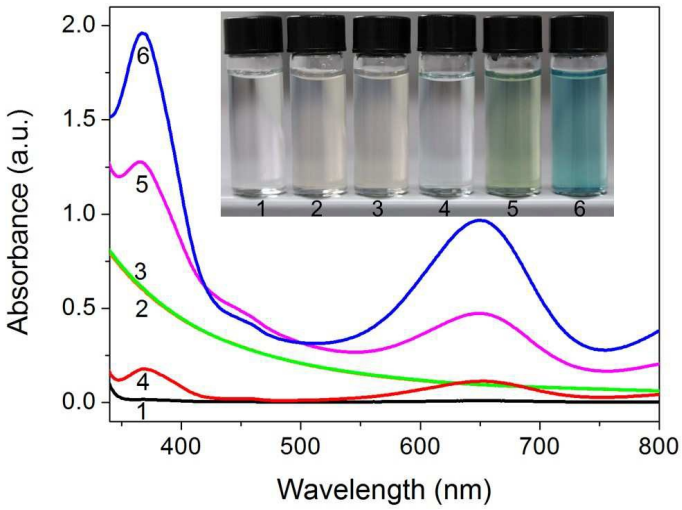

(a)

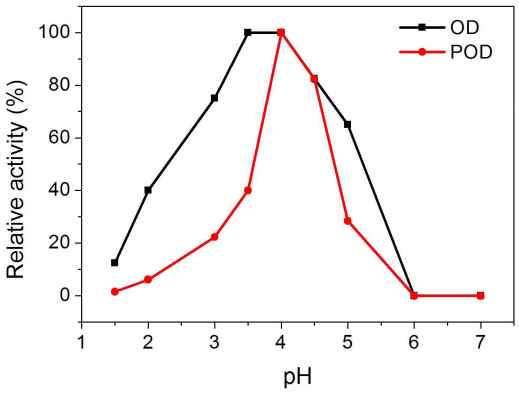

(b)

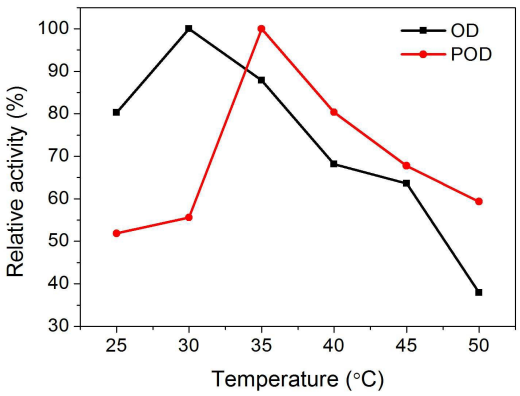

(c)

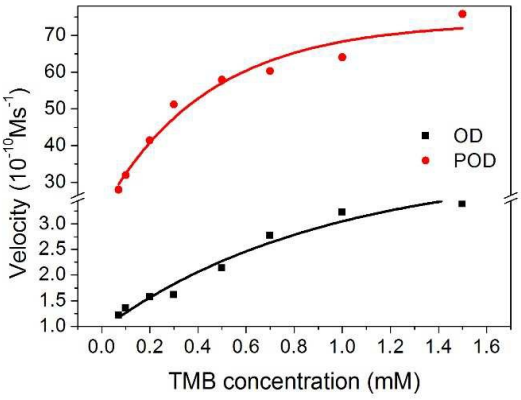

(d)

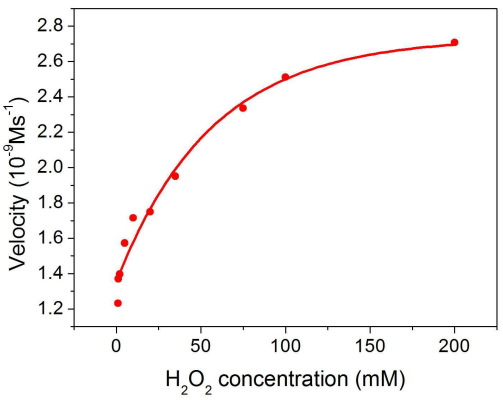

(e)

View Article Online
DOI: 10.1039/C7NR05629J

Figure 3

(a)

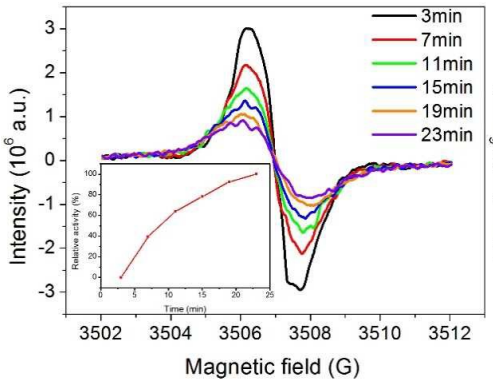

(b)

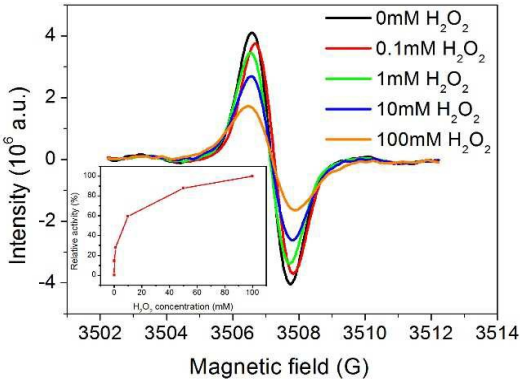

(c)

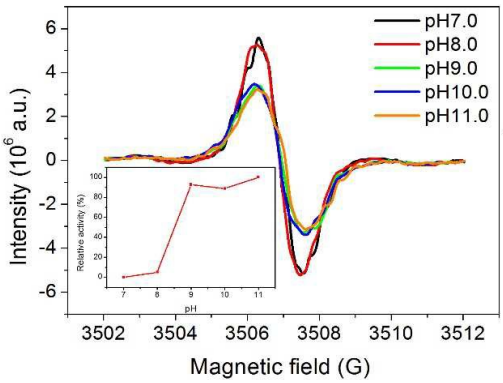

(d)

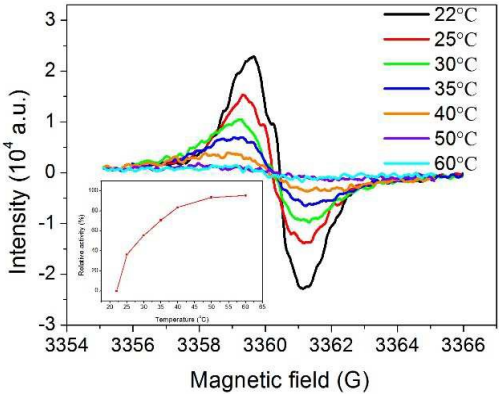

(e)

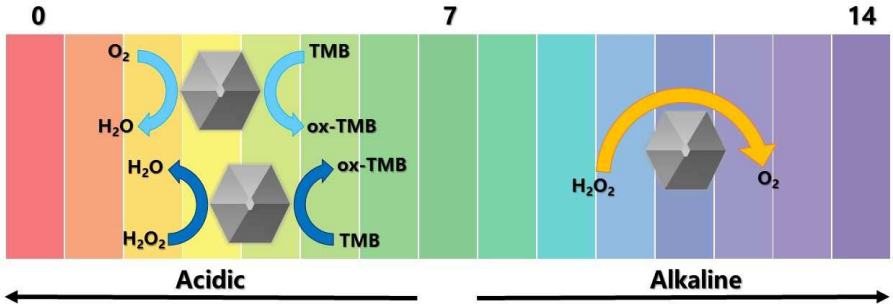

(f)

View Article Online
DOI: 10.1039/C7NR05629J

Figure 4

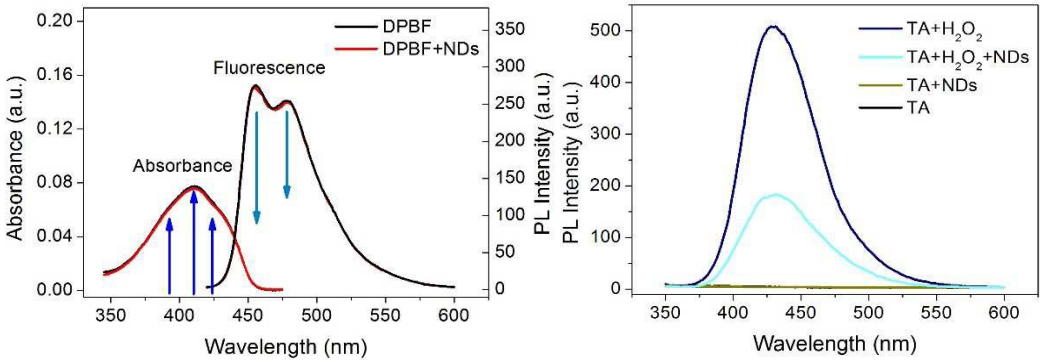

(a) (b)

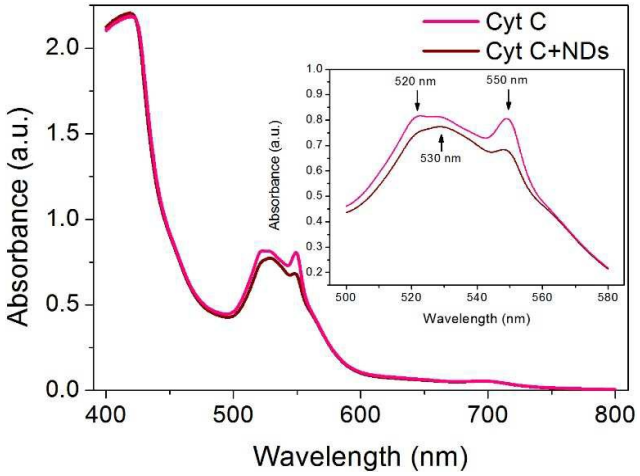

(c)

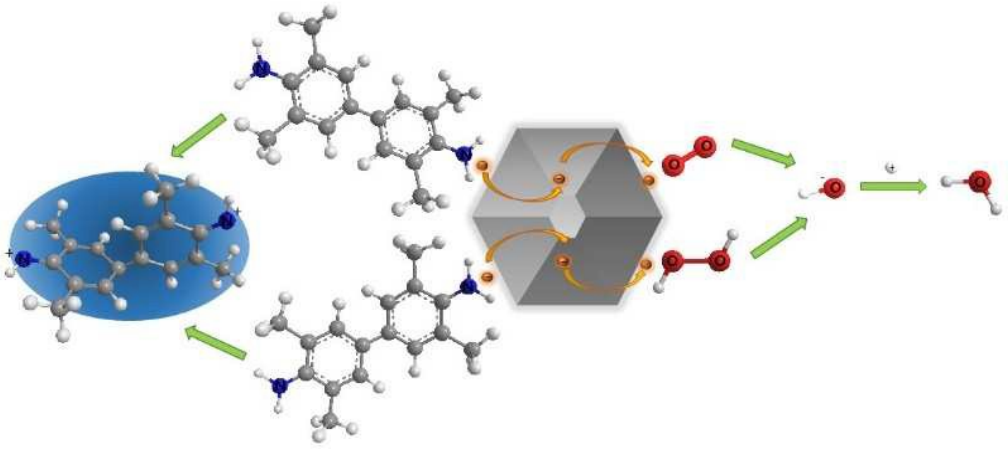

(d)

View Article Online
DOI: 10.1039/C7NR05629J

Figure 5

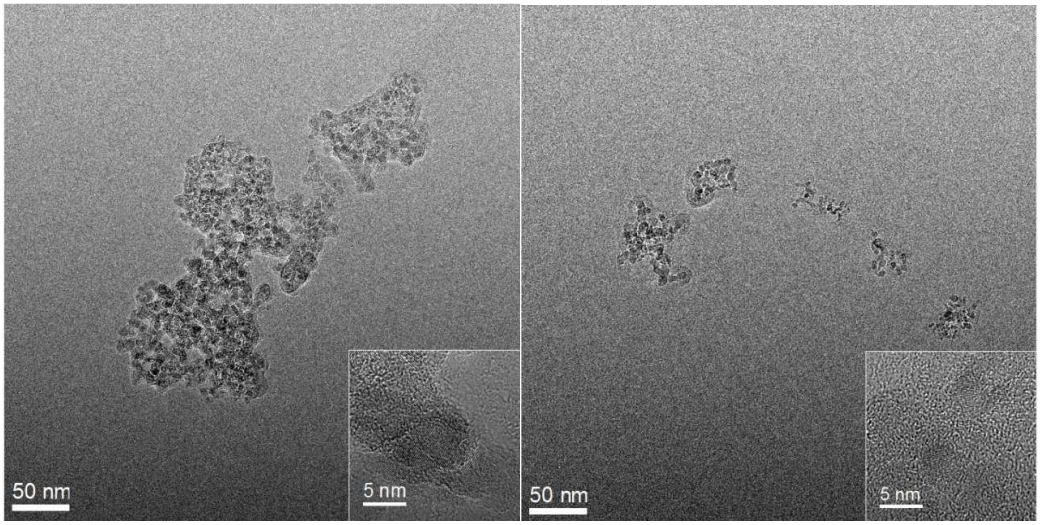

(a) (b)

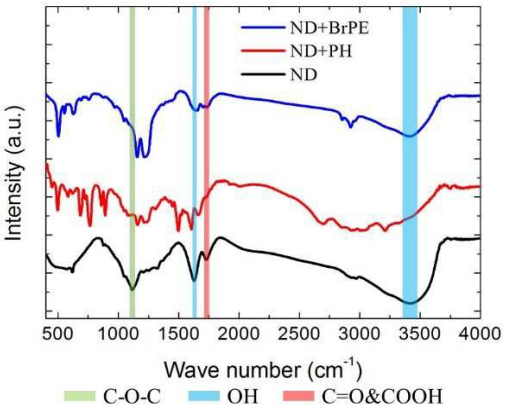

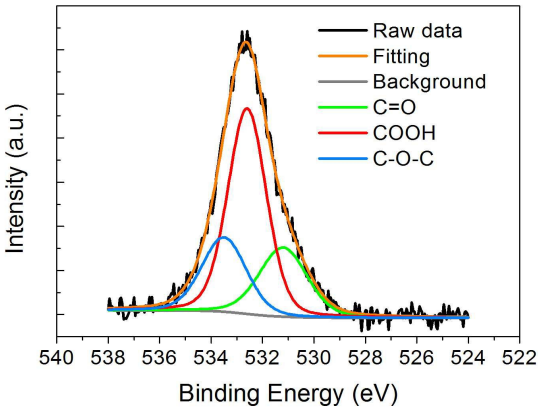

(c) (d)

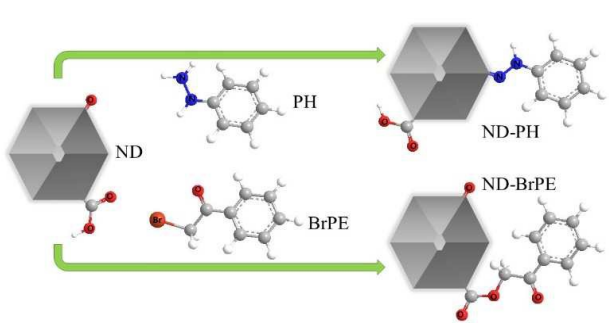

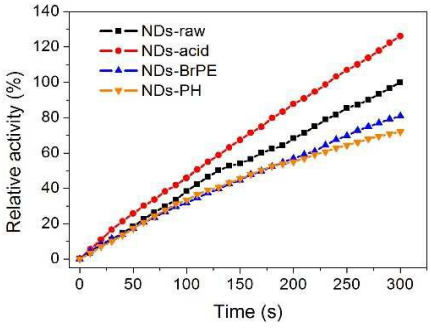

(e) (f)

View Article Online
DOI: 10.1039/C7NR05629J

Figure 6

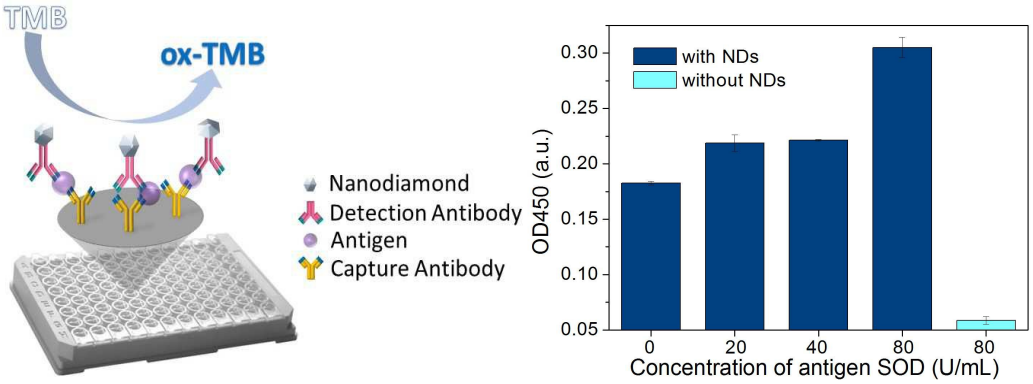

(a) (b)

View Article Online
DOI: 10.1039/C7NR05629J

Figure 7

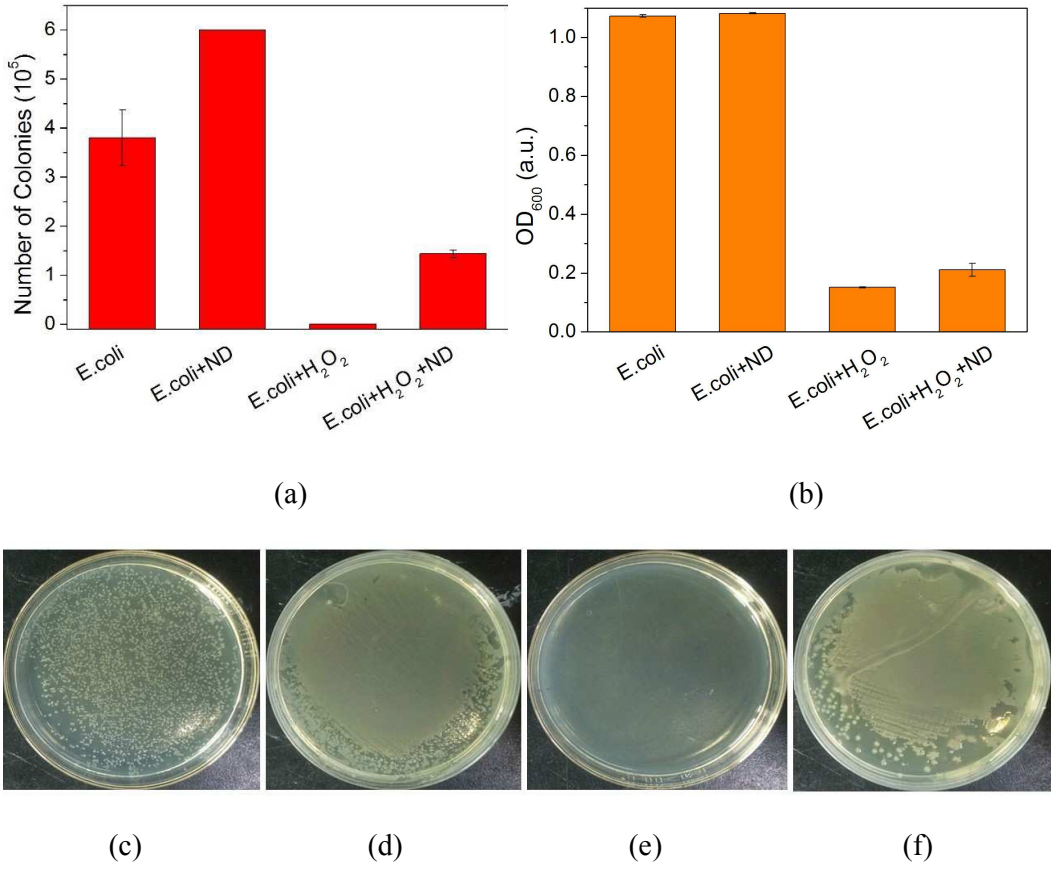

(a) (b)

(c) (d) (e) (f)

View Article Online
DOI: 10.1039/C7NR05629J

TOC

We have demonstrated that nanodiamonds (NDs), as oxidation and reduction catalysts, possess intrinsic enzyme mimetic properties of oxidase, peroxidase and catalase, and these behaviors can be switched by modulating the pH value. Replacing horseradish peroxidase by NDs, an immunosorbent assay was developed for the detection of mouse superoxide dismutase. Meanwhile, the peroxidase-like activity made NDs be an excellent antioxidant against H_2O_2-induced cellular damage.